Catalytic Deoxyribozyme-Modified Nanoparticles for RNAi-Independent Gene Regulation

Kevin Yehl,[†] Jayashree P. Joshi,[‡,§] Brandon L. Greene,[†] R. Brian Dyer,[†] Rita Nahta,[‡,§,⊥] and Khalid Salaita[†,‡,*]

[†]Department of Chemistry, [‡]Winship Cancer Institute, [§]Department of Pharmacology, and [⊥]Department of Hematology and Medical Oncology, Emory University, Atlanta, Georgia 30322, United States

ABSTRACT

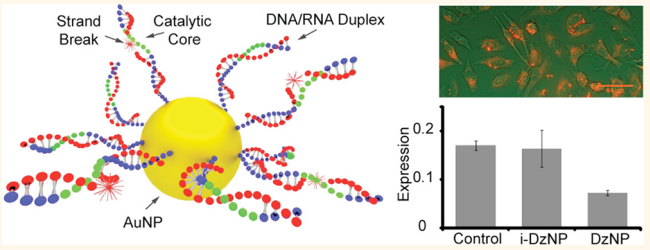

DNAzymes are catalytic oligonucleotides with important applications in gene regulation, DNA computing, responsive soft materials, and ultrasensitive metal-ion sensing. The most significant challenge for using DNAzymes *in vivo* pertains to nontoxic delivery and maintaining function inside cells. We synthesized multivalent deoxyribozyme "10-23" gold nanoparticle (DzNP) conjugates, varying DNA density, linker length, enzyme orientation, and linker composition in order to study the role of the steric environment and gold surface chemistry on catalysis. DNAzyme catalytic efficiency was modulated by steric packing and proximity of the active loop to the gold surface. Importantly, the 10-23 DNAzyme was asymmetrically sensitive to the gold surface and when anchored through the 5′ terminus was inhibited 32-fold. This property was used to generate DNAzymes whose catalytic activity is triggered by thiol displacement reactions or by photoexcitation at $\lambda = 532$ nm. Importantly, cell studies revealed that DzNPs are less susceptible to nuclease degradation, readily enter mammalian cells, and catalytically down-regulate GDF15 gene expression levels in breast cancer cells, thus addressing some of the key limitations in the adoption of DNAzymes for *in vivo* work.

KEYWORDS: deoxyribozyme · DNAzyme · gold nanoparticle · gene regulation · GDF15 · Herceptin · trastuzumab · breast cancer · synthetic biology

Deoxyribozymes (DNAzymes) are catalytic DNA molecules that are widely used in the areas of biocomputational logic gates and circuits (DNA computing),[1] programmable materials,[2] ultrasensitive UO_2^{2+} and Pb^{2+} metal-ion detection,[3,4] for understanding gene function, and as therapeutics.[5] The most commonly used catalytic oligonucleotide, the "10-23" DNAzyme, consists of a 15-base enzymatic core flanked by two arms and functions as a site- and sequence- specific RNase.[6] Consequently, the 10-23 DNAzyme has been tested as a therapeutic in animal models due to its ability to block translation of tumorigenic genes.[7−11]

Gene regulation using DNAzymes is very attractive due to the inherent ease and low cost of synthesis, high selectivity, and significant catalytic efficiency.[12] Moreover, DNAzymes will catalytically inhibit translation in a manner that is independent of RNA interference (RNAi), thus circumventing the need for using a short interfering RNA (siRNA) to hijack the RNA-induced silencing complex.[5,7−11] However, modulating gene expression and transitioning this class of functional nucleic acids *in vivo* will not be possible without solving the issues of cellular delivery and intracellular stability.[12,13] A wide range of sophisticated chemical modifications to the DNAzyme backbone, its nucleic bases, and the secondary structure of its 5′ and 3′ termini increase the intracellular stability of catalytic oligonucleotides to varying degrees, but the challenge of delivery with minimal toxicity is persistent.[14,15]

To address the problem of deploying DNAzymes within cells, we synthesized polyvalent DNAzyme−gold nanoparticle (DzNP) conjugates to generate a nanozyme (Figure 1a and Table S1 in Supporting Information). A nanozyme is typically defined as a self-assembled multivalent catalytic particle that functions as a single entity and that generally displays enhanced substrate binding, stability, and, in some cases, higher activity than the individual catalytic subunits.[16] This mechanism of multienzyme complexes is widely employed in Nature. For example, enzymes are assembled at the lipid membrane or arranged by scaffolding proteins to enhance substrate channeling or alter catalytic activity.[17] Herein, we aimed to investigate DzNPs as a model to investigate how spatial

* Address correspondence to k.salaita@emory.edu.

Received for review July 30, 2012 and accepted September 11, 2012.

Published online September 11, 2012
10.1021/nn3034265

© 2012 American Chemical Society

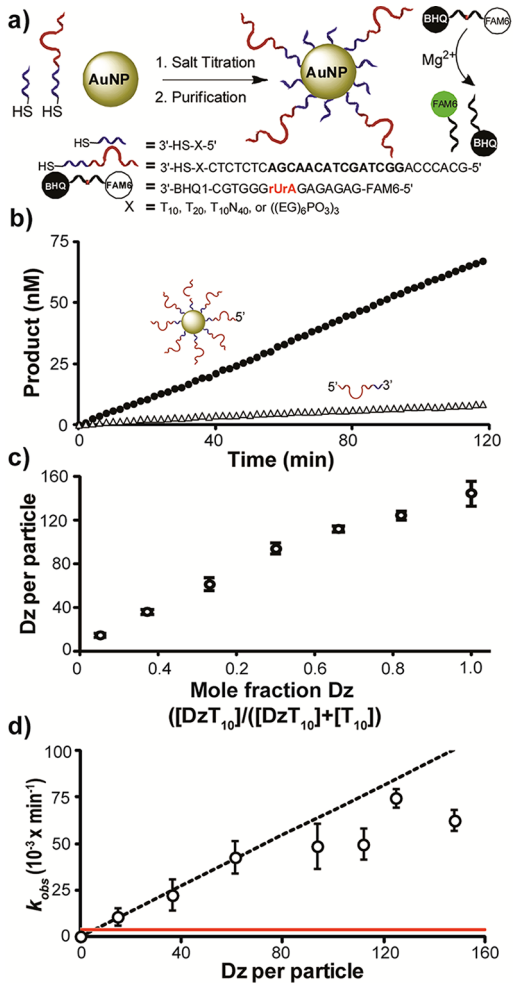

Figure 1. DzNP synthesis and catalysis. (a) Schematic of the strategy used to generate DNAzyme–gold nanoparticle conjugates (DzNPs). A binary mixture of two oligonucleotides, DNAzymes and passivating strands, was used to control the steric environment at the particle surface. The catalytic activity of DzNPs was determined by measuring the rate of fluorescence increase, which represents the rate of substrate hydrolysis and dequenching. (b) Representative kinetic plot showing the rate of catalysis for 4.2 nM DzT_{10}NP ([AuNP] = 4.2 nM) (closed circles) and DzT_{10} (triangles) enzymes ([Mg^{2+}] = 50 mM). (c) Plot showing the DNAzyme surface density for T_{10}-passivated DzNPs as a function of the mole fraction of DNAzyme added during the NP functionalization. (d) Plot showing k_{obs} for the hydrolysis of a series of DzNPs that vary in DNAzyme surface density at [Mg^{2+}] = 10 mM. The horizontal red line denotes the activity of free DzT_{10} (4.2 nM). The diagonal dashed line is a best fit (R^2 = 0.99) through the lower density DzNP data points (≤60 DNAzymes/particle). All error bars represent the standard deviation of three measurements.

organization and nanoparticle confinement affect the properties of enzymes. The DNA–gold nanoparticle conjugate is an attractive platform because the structural conformation of immobilized DNA molecules on gold nanoparticles has been well-characterized and due to the novel properties of these assemblies.[18–20] DNA–gold nanoparticle conjugates are highly stable and have shown successful intracellular gene regulation through antisense and RNAi mechanisms.[21,22] This is due to their enhanced binding affinities,[23] resistance to nuclease degradation,[24] high cellular uptake,[25] and diminished cellular toxicity[26] when compared to free oligonucleotides. DNA–gold nanoparticle conjugates also display highly cooperative hybridization with sharp thermal melting curves when hybridized to complementary DNA gold nanoparticles.[27] Consequently, we rationalized that DzNPs would show superior properties as a gene regulation agent in addition to providing a model platform to explore the fundamental role of supramolecular organization in tuning the catalytic efficiency of nanozymes. We report the synthesis and characterization of 10-23 DzNPs and show that these nanozyme assemblies are sensitive to DNA density and orientation and can catalytically regulate intracellular gene expression through site-selective cleavage of target messenger RNA (mRNA). This work demonstrates a facile route to design, deploy, and trigger DNAzymes within cells.

Very little is known about the structural conformation of the active catalytic loop of DNAzymes. A crystal structure of an inactive 10-23 DNAzyme–substrate complex was solved and showed a Holliday junction conformation (composed of two DNAzymes and two RNA substrates) with dimensions of 50 × 40 × 40 Å.[28] Even though the crystal structure of the active 15-base catalytic loop of the 10-23 DNAzyme is not available, this X-ray structure suggests that severe steric crowding may occur within the context of a high density polyvalent DNA nanoparticle conjugate. Therefore, we sought to determine if the steric environment of an RNA-cleaving DzNP would inhibit catalysis. Previous studies by Lu and co-workers used catalytic RNA-cleaving DNAzyme "8-17" to amplify the reporter signal in analytical assays for transition metals.[3,4,29,30] In those systems, the DNAzyme was hybridized to linker strands that bridged the terminal sequences of DNA-functionalized nanoparticles, and therefore, the DNAzymes were separated from the gold core.[3,4,29,30] Recently, 80 nm iron oxide particles functionalized with 1.6 DNAzymes/particle were synthesized for HCV gene regulation; however, it remains unclear how direct DNAzyme conjugation (or general enzyme conjugation) to the NP surface alters catalytic activity.[31–33]

RESULTS AND DISCUSSION

DzNP Synthesis and Catalysis. In a typical DzNP synthesis, we reduced 3′-thiol-modified oligonucleotides (50 μM), then mixed with gold nanoparticles suspended in phosphate buffered saline (pH 7.4) at a final DNA and particle concentration of 3 μM and 6 nM, respectively. The solution was then stabilized with sodium dodecyl sulfate and salted to 0.7 M NaCl over a period of 3 h with intermittent sonication (Supporting Methods).[34] The oligonucleotide density of the purified DzT_{10}NPs, where T_{10} refers to the thiolated poly T spacer linking the DNAzyme to the nanoparticle, was 160 ± 10

oligonucleotides/particle based on a fluorescence DNA quantification kit (Invitrogen). To verify particle integrity, TEM and UV−vis analysis were performed before and after particle functionalization and indicated that the particles remained dispersed following modification with DNAzymes (Figure S1). The catalytic activity of these particles was determined by measuring the rate of hydrolysis of a diribonucleotide within a DNA substrate that was functionalized with a 5′ 6-fluorescein (FAM6) and a 3′ black hole quencher (BHQ) (Figure 1a and Table S1). This reaction rate was measured using a temperature-controlled fluorometer and reported as k_{obs} using a fluorescence calibration curve for a 3′-FAM6-modified oligonucleotide standard. K_{obs} is defined as the rate of product formation normalized by the enzyme concentration (min^{-1}), which is equal to the DzNP concentration or the soluble DNAzyme concentration in each experiment. Figure 1b shows representative reaction kinetics for DzT_{10}NPs and free DzT_{10} (see Figure 1a for sequences) under identical conditions (25 °C, [DzT_{10}] and [DzT_{10}NP] = 4.2 nM, 1 μM substrate, 20 mM Tris, pH 7.4, 300 mM NaCl, and 50 mM Mg^{2+}). The initial rate of the reaction was determined from the linear slope of the plot (t < 80 min). The k_{obs} values for soluble DzT_{10} and DzT_{10}NP were 0.017 and 0.134 min^{-1}, respectively. In all of our analyses, we chose to compare a DzNP, rather than its individual subunits, to a single DNAzyme molecule in accordance with past literature.[21,23] This is typical because the nanoparticle functions as an ensemble entity inside living cells.[21] For comparison, the individual enzyme subunits in DzNPs showed an activity of 0.0025 min^{-1} when assuming a 33% hybridization efficiency.[35] We also found that DzNPs are stable under these conditions, and particles that were used in catalysis reactions for 12 h only showed a 20% decrease in activity when they were reused the following day (Figure S2). Importantly, these data confirm that the DzNPs are robust and retain catalytic activity despite the dense oligonucleotide environment on the nanoparticle.

Role of Surface Density and Linker Chemistry on Catalysis. To systematically study the effect of surface packing density and steric crowding on the rate of catalysis, a series of DzNPs were synthesized using a binary mixture of two oligonucleotides that included a T_{10} passivating sequence along with the DzT_{10}. In this series, the total ssDNA concentration was kept constant while adjusting the molar concentrations of 3′-thiol-modified DzT_{10} and T_{10}. Because both oligonucleotides have the same T_{10} spacer, the DNA composition of gold nanoparticles was expected to reflect that of the bulk solution.[35] The goal was to tune the average spacing between adjacent DNAzymes and consequently tune steric crowding. The total number of DNA molecules per particle was measured using a commercial fluorescence assay (Figure 1c and Figure S3).[35] To further verify these measurements, DNA was released from the particle surface using dithiothreitol (DTT) and the DNAzyme concentration was determined by using the observed rate constant of substrate hydrolysis as compared to a calibration standard of soluble DNAzyme (Figure S3). Figure 1d shows a plot of the initial rate constant of DzNPs with a range of enzyme packing densities compared to soluble DNAzyme under standard reaction conditions (25 °C, [DzT_{10}NP] = 4.2 nM, 1 μM substrate, 20 mM Tris, pH 7.4, 300 mM NaCl, and 10 mM Mg^{2+}). For direct molecule to molecule comparison, see Figure S4a. We found that at lower enzyme packing densities (15−60 enzymes/particle) the activity of each particle shows a linear increase as a function of the number of DNAzymes per particle. However, particles with packing densities exceeding 60 DNAzymes per particle show saturation in activity. This trend suggests that steric packing limits the maximum activity of each DzNP assembly. As a corollary, this limit in maximum activity equates to each catalytic oligonucleotide requiring a footprint that is at least ~11 nm^2 on the particle surface in order to achieve its maximum activity under these conditions.

Given that the hybridization efficiency and gene regulation efficacy have been shown to be dependent on the chemical nature of the group anchoring an oligonucleotide to a gold nanoparticle, we decided to next investigate the catalytic properties of DzNPs modified with the following poly T and ethylene glycol phosphate linkers: T_{10}, T_{20}, $T_{10}N_{40}$, and $((EG)_6PO_3)_3$ (Table S1). The measured oligonucleotide density of fully packed particles was 148 ± 10, 137 ± 10, 80 ± 1, and 195 ± 2 oligonucleotides/particle for the T_{10}, T_{20}, $T_{10}N_{40}$, and $((EG)_6PO_3)_3$ linkers, respectively. The differences in packing densities were hypothesized to be due to a combination of steric crowding and interaction of the linker nucleobases with the gold surface. Given these DNA densities, we expected that longer linkers would generate DzNPs with increased catalytic efficiency, as this difference would be due to reduced steric inhibition for longer linkers. Surprisingly, no clear trend was observed between k_{obs} and increasing linker length (Figure S4b). In fact, $DzT_{10}N_{40}$NP (0.032 min^{-1}) had a decrease in activity when compared to DzT_{10}NP (0.062 min^{-1}) and DzT_{20}NP (0.062 min^{-1}), which had identical activities (Figures S4b and S5). The ethylene glycol phosphate $((EG)_6PO_3)_3$ linker generated the most densely packed particles (~195 Dz molecules/particle), and when these particles were compared to DzT_{10}NP and DzT_{20}NP, they showed a 56% increase in k_{obs} (Figures S4b and S5). Since polyethylene glycol linkers are known to minimize nonspecific adsorption on surfaces,[34,36] the results suggest that chemisorption of DNAzyme active site nucleobases to the gold surface alters catalytic activity and may play a more significant role in tuning the catalytic activity of DzNPs.

Role of DNAzyme Orientation on Catalytic Activity of DzNP. The role of nonspecific interactions in DzNP catalytic

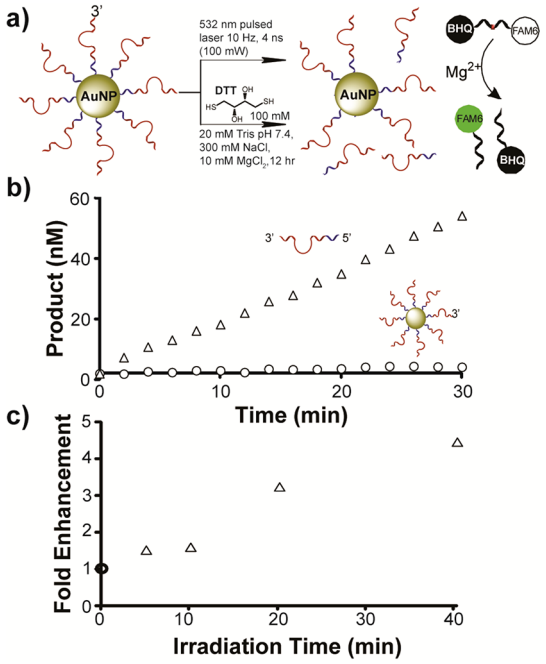

Figure 2. Triggering DNAzyme activity by partial release from the particle surface. (a) Schematic showing DTT displacement (bottom) or laser irradiation (top) to release $Dz_{rev}T_{10}$ from the particle to enhance catalysis. (b) Kinetic plot showing rate of catalysis of $Dz_{rev}T_{10}$NP (open circles) and DTT displaced $Dz_{rev}T_{10}$ (open triangles) from the particle. (c) Plot showing k_{obs} as a function of irradiation time where the rate constant was normalized to particle at $t = 0$ min (open circle). Nd:YAG laser was operated at 10 Hz, 4 ns pulse width, generating 125 mW/cm^2 power.

activity was verified when we measured the rate of substrate hydrolysis using gold nanoparticles functionalized with DNAzymes anchored through a 5′ thiol ($Dz_{rev}T_{10}$) rather than the 3′ terminus anchor. The DNA density on these particles was 180 ± 10 oligonucleotides/particle, but we found that their activity was nearly abolished (Figure 2b and Figure S6). Importantly, $Dz_{rev}T_{10}$NPs remained inactive even when their packing densities were reduced to 90 Dz/NP (~50% packed) either with or without T_{10} passivation (Figure S7). Furthermore, when these particles are treated with mercaptoethanol, the DNAzyme surface density is decreased, but again, the activity of the $Dz_{rev}T_{10}$NPs remained suppressed (Figure S8). When $Dz_{rev}T_{10}$NPs were treated with DTT in order to release the surface-bound DNA (Figure 2a), the free DzT_{10} fully recovered its activity, thus displaying a 3200% increase in catalytic activity (Figure 2b). The drastic difference in activity between DzT_{10}NP and $Dz_{rev}T_{10}$NP (900% difference) (Figure S6) suggests that the catalytic core is asymmetric in its sensitivity to the supporting gold nanoparticle surface.[37] This observation agrees with systematic mutagenesis analysis studies on the 10-23 DNAzyme catalytic domain that has shown a high degree of sensitivity at many bases near the 5′ terminus of the active site.[38] Therefore, DNAzyme orientation needs to be carefully examined in DzNP design, which should be a general consideration that is broadly relevant to other biological nanozymes.

Chemical or Light-Triggered Activation of DNAzymes. Photodynamic control of gene regulation agents, such as DNAzymes, is a highly desirable property, and various synthetic strategies have been employed to demonstrate this capability.[39−41] Because the gold nanoparticle was found to significantly inhibit the DNAzyme anchored through its 5′ terminus, we thought that photoinduced DNA release would be a suitable proof-of-concept to demonstrate a triggered catalytic function (Figure 2a). We released $Dz_{rev}T_{10}$ from the particle by irradiation with a 532 nm pulsed laser, which is known to selectively cleave the thiol−gold bond at certain laser powers (Figure 2c).[42] Importantly, this strategy offers significant advantages because it is synthetically facile and compatible with two-photon and visible irradiation, in contrast to the recently developed azo-benzene and caged-nucleotide based approaches that require excitation at UV wavelengths.[43,44]

DzNPs Can Readily Enter Cells and Regulate Gene Expression. Having shown that properly designed DzNPs are catalytically active in buffer conditions, we next set out to investigate their activity under conditions that mimic the cellular environment by exposing the particles to nucleases and serum. To test DzNP resistance toward nucleases, the catalytic activity of free DzT_{10} and DzT_{10}NP was measured before and after incubation with a model nuclease, DNase I. Figure 3a shows that, after DNase I treatment (120 min), the soluble enzyme retained only 10% of its original activity, while the DzNPs retained 90% of its original activity. This result is in agreement with previous reports showing that polyvalent DNA-modified gold nanoparticles shield oligonucleotides from hydrolytic cleavage by DNases.[24] We also tested the activity of DzNPs that are exposed to 10% fetal bovine serum for 24 h and found the particles to remain active (Figure S9).

To determine whether DzNPs enter mammalian cells and catalytically regulate gene expression, we designed DzNPs with recognition arms specific toward the TGF-β related growth differentiation factor 15 (GDF15) mRNA sequence (Dz_{GDF15}NP, Table S1).[45] GDF15 was selected as a proof-of-concept due to its clinical association with disease progression and resistance to chemotherapy in breast, prostate, ovarian, and colorectal cancer, and its knockdown has been shown to inhibit proliferation.[46−48] Moreover, GDF15 is found to contribute, in part, to the development of resistance to the anti-HER2 therapeutic trastuzumab (Herceptin, Genetech, Inc.).[49] HER2 is overexpressed in approximately 20−30% of metastatic breast cancers, and trastuzumab is the first line of treatment for this subset of tumors. Acquired resistance to trastuzumab will typically develop in patients within one year of therapy.[50] Moreover, viral vector-based knockdown of GDF15 has been shown to rescue some of the sensitivity to trastuzumab in breast cancer

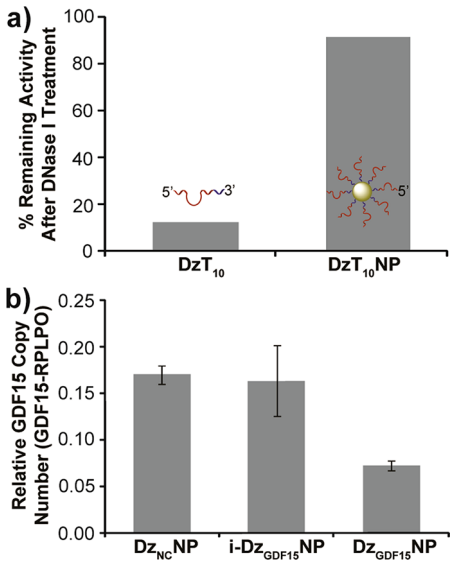

Figure 3. Gene regulation using DzNP. (a) Bar graph showing the relative catalytic activity of DzT_{10} and DzT_{10}NP after exposure to DNase I for 120 min at 37 °C. (b) Real-time PCR analysis of GDF15 mRNA expression of HCC1954 cells, which were treated with catalytic (Dz_{GDF15}NP) and noncatalytic (i-Dz_{GDF15}NP) DzNPs targeting GDF15 mRNA and nonspecific catalytic (Dz_{NC}NP) DzNPs at a concentration of 5 nM for 48 h. The catalytic particles down-regulated GDF15 mRNA ~57% relative to nonspecific particles ($p < 0.005$).

cell line models that acquire resistance.[49] These results provide the therapeutic rationale for targeting GDF15.

The GDF15-specific DNAzyme included two 2′-O-methyl RNA bases that were incorporated within both the 5′ and 3′ termini, which is a common modification to reduce nuclease degradation in cell studies.[21] To distinguish between antisense and DNAzyme-catalyzed hydrolysis mechanisms, we introduced a single base mutation in the DNAzyme catalytic core (G1 to A1) to generate catalytically inactive nanoparticles (i-Dz_{GDF15}NP, Table S1).[6,38] Negative control particles (Dz_{NC}NP) were also synthesized, and their DNA sequences included two randomized N8 arms flanking the 15-mer catalytic loop to control for off-target effects (Table S1). The oligonucleotide density was quantified in these three types of particles and found to be 200 ± 10, 230 ± 40, and 111 ± 10 DNAzymes per particle for i-Dz_{GDF15}NP, Dz_{GDF15}NP, and Dz_{NC}NP, respectively. After confirming that DzNPs readily enter mammalian cells (Figure S10), HCC1954 HER2-overexpressing breast cancer cells were treated with 5 nM of particles for 48 h, and then analyzed using real-time PCR to quantify GDF15 mRNA expression levels relative to the housekeeping gene RPLPO (component of the 60S ribosomal subunit). The dosage of 5 nM particles was selected since the 20 nM dose showed some toxicity under these conditions (results not shown). The average GDF15 expression levels relative to RPLPO are shown in Figure 3b and are reported as relative GDF15 copy number ($2\Delta C_t$). The error represents the standard error of the mean (SEM) and was calculated from three independent experiments, where each experiment generally consisted of three wells and the PCR expression level within each well was measured three times. ANOVA statistical analysis was performed on the data and indicates that the enzymatic nanoparticles, Dz_{GDF15}NP, reduce GDF15 expression by ~57% relative to negative control particles with a p value less than 0.005, whereas i-Dz_{GDF15}NPs showed an average of ~4% knockdown, similar to reported literature values for antisense oligonucleotides gold nanoparticles[21] but was within experimental error of Dz_{NC}NPs. Since both types of DNA-modified nanoparticles are complementary to the GDF15 mRNA, they are expected to reduce GDF15 expression levels through a common antisense mechanism, and the difference in the activity between active and inactive nanoparticles can be attributed to the contributions of the catalytic oligonucleotides. Optimized lentiviral shRNA-based knockdown of GDF15 in this cell lines has been reported to display a ~50% reduction in GDF15 expression as measured by PCR,[49] which is comparable to the efficacy of 5 nM Dz_{GDF15}NPs.

CONCLUSION

We generated DNAzyme "10-23" NPs and determined some of the design parameters that control catalysis, such as loading density, linker length, linker composition, and DNAzyme orientation. These rules will guide the design of enzymatic DNA nanomaterials, thus providing a new direction in the growing field of DNAzyme-based therapeutics as new catalytic oligonucleotides are discovered. We demonstrate that DzNPs can knockdown GDF15 expression through a catalytic mechanism of action within cells in an RNA interference-independent pathway. Given that DNAzyme function is complementary to that of siRNA-based gene regulation, there is potential in a dual DzNP and siRNA-NP strategy and especially if one intends to target genes that regulate RISC function. The ability to incorporate DNAzyme-based computing, metal-ion and small-molecule sensing inside a cell will provide new opportunities in synthetic biology.

MATERIALS AND METHODS

Synthesis of Gold Nanoparticles. Citrate-stabilized gold nanoparticles (14 ± 1.6 nm) were prepared using published procedures.[51] A 500 mL solution of 1 mM hydrogen tetrachloroaurate(III) trihydrate solution was brought to a vigorous boil, and once boiling, 50 mL of a 38.8 mM sodium citrate tribasic dihydrate solution was added and allowed to reflux for 15 min. The reaction mixture was filtered using a 0.45 μm acetate filter, producing monodisperse AuNPs. The resonance wavelength of the gold nanoparticles was determined using UV–vis spectrometry, and particle size was determined using transmission electron microscopy (TEM).

Preparation of Deoxyribozyme-Functionalized Gold Nanoparticles. Disulfide-modified oligonucleotides at either the 5′ or 3′ end were purchased from Integrated DNA Technologies (IDT). The disulfide was reduced to a free thiol by incubating 35 nmols of lyophilized oligonucleotide with 700 μL of disulfide cleavage buffer (0.1 M dithiothreitol (DTT), 170 mM phosphate buffer at pH 8.0) for 3 h at room temperature. The reduced oligonucleotides were purified using a NAP-25 column (GE Healthcare, Piscataway, NJ) with Nanopure water as the eluent. Subsequently, 30 nmol of DNA was added to 7.5 mL of 14 nm gold nanoparticles (10 nM), bringing the final concentration of oligonucleotide and gold nanoparticles to ~3.2 μM and ~7.3 nM, respectively. The pH of the solution was adjusted to pH 7.4 by adding 93.8 μL of 100 mM phosphate buffer, thus bringing the phosphate buffer concentration to 9 mM. The particles were stabilized by adding sodium dodecyl sulfate (SDS) to the solution and bringing its final concentration to 0.1% (g/mL) by using a stock solution of 10% SDS. The particles were successively salted with eight NaCl additions that were spaced 20 min apart using a stock solution of 2.0 M NaCl and 10 mM phosphate buffer. The final NaCl concentration of the DNA−AuNP solution was increased to 0.7 M. The first two NaCl additions increased the concentration by 0.05 M increments, while the remaining six NaCl additions increased the NaCl concentration by 0.1 M increments. The particles were immediately sonicated for 10 s after each salt addition to maximize DNA packing, as indicated in literature protocols.[34] The fully salted particles were then incubated overnight, in the dark and at room temperature. We found that the 10-23 active catalytic core of the DNAzyme had a tendency to drive the formation of nanoparticle aggregates at 0.7 M NaCl due to partial self-complementarity of sequences. The formation of these aggregates did not result in any observable reduction in the quality of the particles (as measured by UV−vis, TEM, catalysis, DNA density). The following day, the particles were centrifuged four times, reconstituted in Nanopure water each time, and stored at 4 °C for future use for a maximum duration of 1 month.

TEM Imaging of DzNPs. Transmission electron microscopy samples were prepared by pipetting an 8 nM gold nanoparticle solution onto a TEM grid. TEM was conducted on a JEOL JEM-1210 transmission electron microscope. The mean nanoparticle diameter was used to obtain the extinction coefficient, and particle concentrations were subsequently determined using a NanoDrop 2000C spectrophotometer.

Calculation of the Number of Deoxyribozyme Molecules per AuNP. The commercial Quant-iT OliGreen ssDNA kit or measuring the rate of hydrolysis of a quenched substrate by released DNAzyme was used to determine the total DNA or DNAzyme density per particle. Both methods yield comparable oligonucleotide concentration values. The Quant-iT OliGreen ssDNA kit required preparing a calibration curve by diluting a DNA stock solution (4 μg/mL) composed of the same thiolated oligonucleotides that were used during particle functionalization to 0.1, 0.2, 0.5, 0.75, 1, and 2 μg/mL and a final volume of 100 μL in TE buffer. DzNP solutions were prepared by diluting an 8 nM stock solution to 0.4, 0.6, and 0.8 nM with TE buffer. The Dz oligonucleotides were released from the particle through oxidizing/dissolving the gold with potassium cyanide (KCN) by adding 1 μL of a 5 M stock solution of KCN to each well, including the calibration wells to be consistent. The solutions were incubated with KCN for 30 min to ensure complete dissolution. After complete dissolution of the gold nanoparticles, 100 μL of the freshly prepared 1× Quant-iT OliGreen solution was added to each well and fluorescence intensities (485/528 nm excitation/emission) of each well were then measured using a Bio-Tek Synergy HT plate reader to determine the total DNA density. The DNAzyme density was calculated assuming that the DNA ratio on the particle was the same as that in solution during the functionalization process. To confirm the oligonucleotide density per AuNP values that were measured using the Quant-iT assay, DNAzyme concentrations were determined by using the observed rate constant of substrate hydrolysis as compared to a calibration standard of soluble DNAzyme. Oligonucleotides were released from the particle surface by incubating 1 nM DzNP solutions with 100 mM DTT for 5 h. After incubation, catalysis buffer was added (20 mM Tris, pH 7.4, 300 mM NaCl, and 10 mM $MgCl_2$) along with 1 μM substrate, and initial rates of catalysis were measured (as described below). The initial rates were compared to a calibration curve of free DNAzyme activity that was measured under identical reaction conditions.

Measurement of DzNP Activity. DNAzyme catalytic activity was determined by measuring the fluorescence intensity as a function of time, which indicated the rate of hydrolysis of a DNA/RNA chimera substrate that was functionalized with a 5′ 6-fluorescein (FAM6) and a 3′ black hole quencher (BHQ). Fluorescence was measured using a temperature-controlled Bio-Tek Synergy HT plate reader. All experiments were conducted under the same reaction conditions unless otherwise stated: 25 °C, 4.2 nM Dz or DzNP, 1 μM substrate, 20 mM Tris, pH 7.4, 300 mM NaCl, and 10 mM $MgCl_2$. The rate constant of product formation was quantified in units of mol min^{-1} by using a fluorescence calibration curve for a 3′-FAM6-modified oligonucleotide standard that included 4.2 nM DNA-modified AuNPs to account for the strong NP absorbance at λ = 520 nm (Calibration Probe, Table S1). The initial rate of the reaction was determined from the initial slope of the plot (t < 80 min). During catalysis, it was observed that, only in the presence of both substrate and 10 mM Mg^{2+}, DzNPs formed aggregates that settled to the bottom of the reaction vessel. We believe that this is due to a non-cross-linking DNA hybridization aggregation phenomenon, which was reported previously.[52] To verify that these aggregates are the catalytic entity responsible for catalysis, the reaction solution was exchanged and catalysis was subsequently measured. Very little change in rates was observed, indicating that DNAzyme−gold nanoparticle conjugates remain anchored to the gold nanoparticle surface (Figure S3).

Determination of Nuclease Resistance. DNase I was acquired from New England BioLabs, Inc. and used as indicated by the manufacturer. DNase I was incubated with 1.9 μM DzT_{10} and 10.4 nM DzT_{10}NP (DzT_{10} = 1.9 μM) at a DNase I concentration of 2.5 units/mL in 1× DNase I reaction buffer (10 mM Tris-HCl, pH 7.6, 2.5 mM $MgCl_2$, and 0.5 mM $CaCl_2$) with a final volume of 40 μL at 37 °C for 2 h. Afterward, DNase I was inactivated by heating to 75 °C for 10 min. Tris (pH 7.4), NaCl, substrate, and $MgCl_2$ were then added, thus bringing the total volume to 150 μL and replicating the standard reaction conditions (except [DzT_{10}] = 500 nM). Retention of activity was measured by normalizing the enzymatic activity to the DNAzyme activities prior to addition of DNase I under identical conditions.

Cell Culture and DzNP Gene Knockdown. HCC1954 (CRL 2338) cells were obtained from ATCC and were maintained in RPMI supplemented with 10% FBS and 1% penicillin-streptomycin in standard culture conditions (37 °C, 5% CO_2). Cells were seeded in a 12-well plate at a concentration of 30 000 cells/well and were allowed to adhere overnight under standard cell culture conditions. Nanoparticles were sterilized by filtering through a 0.2 μm filter prior to addition to the cell media. To achieve the desired nanoparticle concentration, the filtered particles were centrifuged at high speed (13 200 rpm) for 40 min and then resuspended in a known volume of complete RPMI medium. Five nanomolar Dz−gold nanoparticle solution was allowed to incubate with the cells for 48 h. The medium containing particles was subsequently removed, and the cells were gently washed with PBS. This procedure was repeated twice to remove any potential remaining residual traces of nanoparticles. Total RNA was then isolated using an RNA isolation kit (Sigma, Cat.# RTN-70) and used following the manufacturer's instructions. A total of 48 ng of RNA was used to synthesize cDNA using the Qiagen Sensiscript cDNA synthesis kit (Cat #205213). Real-time PCR was performed using Taqman gene expression primers for GDF15 (Cat.# Hs00171132_m1) and housekeeping gene, RPLPO (Cat.# 433761-1006022) from Applied Biosystems. The data were analyzed using the ΔC_t method and reported as such.

Chemical Activation of DNAzyme Catalytic Activity (Thiol Displacement). A 1 M stock solution of DTT was freshly prepared for each experiment prior to DTT release of DNAzymes from the AuNP. DzNPs were diluted in a 96-well plate to 4.7 nM in reaction buffer (not including substrate). DTT was subsequently added, bringing the final DTT concentration to 100 mM. The particles were incubated in this solution for 12 h. The substrate was added the following day in

order to initiate catalysis. Note that the final DzNP concentration was 4.2 nM which matched the standard catalysis conditions described above.

Photothermal Activation of DNAzyme Catalytic Activity. A 100 μL aliquot of DzNPs at a 2 nM concentration was added to a glass-bottom 96-well SensoPlate (Greiner Bio-One) (O.D. = 0.32). The samples were then irradiated by a frequency-doubled Q-switched Nd:YAG laser (Spectra-Physics) operating at 532 nm with a pulse width of 10 ns and a repetition rate of 10 Hz for 0, 5, 10, 20, and 40 min. The power density was determined using a power meter (Melles Griot) by measuring the power of the unattenuated beam, then attenuating the beam to 50% power using an iris where the beam diameter is approximately equal to the diameter of the iris at half-maximum power. This power density was determined to be 125 mW/cm^2. The optical density of the samples was inferred from the well plate fill level (*i.e.*, path length) and relative nanoparticle concentrations with known extinction coefficients at 532 nm (3.464×10^8 cm^{-1} M^{-1}) at approximately 0.32 O.D., which ensured uniform sample irradiation. After illumination, the activity of the released DNAzyme was measured by adding 1 μM substrate and reaction buffer (20 mM Tris, pH 7.4, 300 mM NaCl, and 10 mM $MgCl_2$) and measuring the initial rate of substrate hydrolysis.

Mercaptoethanol (ME) Passivation of DzNPs. $Dz T_{10}$NP and $Dz_{rev}T_{10}$NP (6 nM) were passivated with ME (12 mM) for 5 and 15 min, respectively, in Nanopure water. After incubation, the particles were washed six times by centrifuging the particles for 10 min at 13 500 rpm into pellets, decanting the supernatant, and resuspending in Nanopure water. The DNAzyme surface density was measured as described above (DNA density assay). Catalysis was measured at the following reaction conditions: 25 °C, 0.75 nM DzNP, 1 μM substrate, 20 mM CHES, pH 8.6, 150 mM NaCl, and 50 mM $MgCl_2$.

Conflict of Interest: The authors declare no competing financial interest.

Acknowledgment. K.S. would like to acknowledge support from the National Institutes of Health (NIH) through R01-GM097399-01, NHLBI Program Excellence in Nanotechnology (HHSN268201000043C), and the Emory University Research Committee (URC) 00016401. R.N. acknowledges support as a Georgia Cancer Coalition Distinguished Scholar. We would like to acknowledge Daniel Stabley for the design of the DzNP graphic in the TOC. The TEM was performed with the support of Ms. Hong Yi and Chunfu Xu at the Robert P. Apkarian Integrated Electron Microscopy Core of Emory University.

Supporting Information Available: Additional experimental details. This material is available free of charge *via* the Internet at http://pubs.acs.org.

REFERENCES AND NOTES

1. Elbaz, J.; Lioubashevski, O.; Wang, F. A.; Remacle, F.; Levine, R. D.; Willner, I. DNA Computing Circuits Using Libraries of DNAzyme Subunits. *Nat. Nanotechnol.* **2010**, *5*, 417–422.
2. Chien, M. P.; Thompson, M. P.; Gianneschi, N. C. DNA-Nanoparticle Micelles as Supramolecular Fluorogenic Substrates Enabling Catalytic Signal Amplification and Detection by DNAzyme Probes. *Chem. Commun.* **2011**, *47*, 167–169.
3. Lee, J. H.; Wang, Z. D.; Liu, J. W.; Lu, Y. Highly Sensitive and Selective Colorimetric Sensors for Uranyl (UO_2^{2+}): Development and Comparison of Labeled and Label-Free DNAzyme-Gold Nanoparticle Systems. *J. Am. Chem. Soc.* **2008**, *130*, 14217–14226.
4. Mazumdar, D.; Liu, J. W.; Lu, G.; Zhou, J. Z.; Lu, Y. Easy-To-Use Dipstick Tests for Detection of Lead in Paints Using Non-Cross-Linked Gold Nanoparticle-DNAzyme Conjugates. *Chem. Commun.* **2010**, *46*, 1416–1418.
5. Fokina, A. A.; Meschaninova, M. I.; Durfort, T.; Venyaminova, A. G.; Francois, J. C. Targeting Insulin-like Growth Factor I with 10-23 DNAzymes: 2′-O-Methyl Modifications in the Catalytic Core Enhance mRNA Cleavage. *Biochemistry* **2012**, *51*, 2181–2191.
6. Santoro, S. W.; Joyce, G. F. A General Purpose RNA-Cleaving DNA Enzyme. *Proc. Natl. Acad. Sci. U.S.A.* **1997**, *94*, 4262–4266.
7. Niewiarowska, J.; Sacewicz, I.; Wiktorska, M.; Wysocki, T.; Stasikowska, O.; Wagrowska-Danilewicz, M.; Cierniewski, C. S. DNAzymes to Mouse Beta 1 Integrin mRNA *in Vivo*: Targeting the Tumor Vasculature and Retarding Cancer Growth. *Cancer Gene Ther.* **2009**, *16*, 713–722.
8. Elahy, M.; Dass, C. R. Dz13: c-Jun Downregulation and Tumour Cell Death. *Chem. Biol. Drug Des.* **2011**, *78*, 909–912.
9. Fahmy, R. G.; Dass, C. R.; Sun, L. Q.; Chesterman, C. N.; Khachigian, L. M. Transcription Factor Egr-1 Supports FGF-Dependent Angiogenesis during Neovascularization and Tumor Growth. *Nat. Med.* **2003**, *9*, 1026–1032.
10. Mitchell, A.; Dass, C. R.; Sun, L. Q.; Khachigian, L. M. Inhibition of Human Breast Carcinoma Proliferation, Migration, Chemoinvasion and Solid Tumour Growth by DNAzymes Targeting the Zinc Finger Transcription Factor EGR-1. *Nucleic Acids Res.* **2004**, *32*, 3065–3069.
11. Zhou, J.; Yang, X. Q.; Xie, Y. Y.; Zhao, X. D.; Jiang, L. P.; Wang, L. J.; Cui, Y. X. Inhibition of Respiratory Syncytial Virus of Subgroups A and B Using Deoxyribozyme DZ1133 in Mice. *Virus Res.* **2007**, *130*, 241–248.
12. Dass, C. R.; Choong, P. F. M.; Khachigian, L. M. DNAzyme Technology and Cancer Therapy: Cleave and Let Die. *Mol. Cancer Ther.* **2008**, *7*, 243–251.
13. Baum, D. A.; Silverman, S. K. Deoxyribozymes: Useful DNA Catalysts *in Vitro* and *in Vivo*. *Cell. Mol. Life Sci.* **2008**, *65*, 2156–2174.
14. Schubert, S.; Gul, D. C.; Grunert, H. P.; Zeichhardt, H.; Erdmann, V. A.; Kurreck, J. RNA Cleaving '10-23' DNAzymes with Enhanced Stability and Activity. *Nucleic Acids Res.* **2003**, *31*, 5982–5992.
15. Abdelgany, A.; Wood, M.; Beeson, D. Hairpin DNAzymes: A New Tool for Efficient Cellular Gene Silencing. *J. Gene Med.* **2007**, *9*, 727–738.
16. Manea, F.; Houillon, F. B.; Pasquato, L.; Scrimin, P. Nanozymes: Gold-Nanoparticle-Based Transphosphorylation Catalysts. *Angew Chem., Int. Ed.* **2004**, *43*, 6165–6169.
17. Miles, E. W.; Rhee, S.; Davies, D. R. The Molecular Basis of Substrate Channeling. *J. Biol. Chem.* **1999**, *274*, 12193–12196.
18. Park, S.-J.; Lazarides, A. A.; Storhoff, J. J.; Pesce, L.; Mirkin, C. A. The Structural Characterization of Oligonucleotide-Modified Gold Nanoparticle Networks Formed by DNA Hybridization. *J. Phys. Chem. B* **2004**, *108*, 12375–12380.
19. Pellegrino, T.; Sperling, R. A.; Alivisatos, A. P.; Parak, W. J. Gel Electrophoresis of Gold-DNA Nanoconjugates. *J. Biomed. Biotechnol.* **2007**, 26796–26804.
20. Macfarlane, R. J.; Lee, B.; Jones, M. R.; Harris, N.; Schatz, G. C.; Mirkin, C. A. Nanoparticle Superlattice Engineering with DNA. *Science* **2011**, *334*, 204–208.
21. Rosi, N. L.; Giljohann, D. A.; Thaxton, C. S.; Lytton-Jean, A. K. R.; Han, M. S.; Mirkin, C. A. Oligonucleotide-Modified Gold Nanoparticles for Intracellular Gene Regulation. *Science* **2006**, *312*, 1027–1030.
22. Giljohann, D. A.; Seferos, D. S.; Prigodich, A. E.; Patel, P. C.; Mirkin, C. A. Gene Regulation with Polyvalent siRNA-Nanoparticle Conjugates. *J. Am. Chem. Soc.* **2009**, *131*, 2072–2073.
23. Lytton-Jean, A. K. R.; Mirkin, C. A. A Thermodynamic Investigation into the Binding Properties of DNA Functionalized Gold Nanoparticle Probes and Molecular Fluorophore Probes. *J. Am. Chem. Soc.* **2005**, *127*, 12754–12755.
24. Wang, H. B.; Xu, W.; Zhang, H.; Li, D. W.; Yang, Z. Q.; Xie, X. J.; Li, T. H.; Liu, X. G. EcoRI-Modified Gold Nanoparticles for Dual-Mode Colorimetric Detection of Magnesium and Pyrophosphate Ions. *Small* **2011**, *7*, 1987–1992.
25. Xie, X; Xu, W.; Liu, X. Improving Colorimetric Assays through Protein Enzyme-Assisted Gold Nanoparticle Amplification. *Acc. Chem. Res.* **2012**, 10.1021/ar300044j.
26. Seferos, D. S.; Prigodich, A. E.; Giljohann, D. A.; Patel, P. C.; Mirkin, C. A. Polyvalent DNA Nanoparticle Conjugates Stabilize Nucleic Acids. *Nano Lett.* **2009**, *9*, 308–311.

27. Giljohann, D. A.; Seferos, D. S.; Patel, P. C.; Millstone, J. E.; Rosi, N. L.; Mirkin, C. A. Oligonucleotide Loading Determines Cellular Uptake of DNA-Modified Gold Nanoparticles. *Nano Lett.* **2007**, *7*, 3818–3821.
28. Massich, M. D.; Giljohann, D. A.; Seferos, D. S.; Ludlow, L. E.; Horvath, C. M.; Mirkin, C. A. Regulating Immune Response Using Polyvalent Nucleic Acid-Gold Nanoparticle Conjugates. *Mol. Pharmaceutics* **2009**, *6*, 1934–1940.
29. Taton, T. A.; Mirkin, C. A.; Letsinger, R. L. Scanometric DNA Array Detection with Nanoparticle Probes. *Science* **2000**, *289*, 1757–1760.
30. Nowakowski, J.; Shim, P. J.; Prasad, G. S.; Stout, C. D.; Joyce, G. F. Crystal Structure of an 82-Nucleotide RNA-DNA Complex Formed by the 10-23 DNA Enzyme. *Nat. Struct. Biol.* **1999**, *6*, 151–156.
31. Liu, J. W.; Lu, Y. A Colorimetric Lead Biosensor Using DNAzyme-Directed Assembly of Gold Nanoparticles. *J. Am. Chem. Soc.* **2003**, *125*, 6642–6643.
32. Wang, Z. D.; Lee, J. H.; Lu, Y. Label-Free Colorimetric Detection of Lead Ions with a Nanomolar Detection Limit and Tunable Dynamic Range by Using Gold Nanoparticles and DNAzyme. *Adv. Mater.* **2008**, *20*, 3263–3267.
33. Ryoo, S. R.; Jang, H.; Kim, K. S.; Lee, B.; Kim, K. B.; Kim, Y. K.; Yeo, W. S.; Lee, Y.; Kim, D. E.; Min, D. H. Functional Delivery of DNAzyme with Iron Oxide Nanoparticles for Hepatitis C Virus Gene Knockdown. *Biomaterials* **2012**, *33*, 2754–2761.
34. Hurst, S. J.; Lytton-Jean, A. K. R.; Mirkin, C. A. Maximizing DNA Loading on a Range of Gold Nanoparticle Sizes. *Anal. Chem.* **2006**, *78*, 8313–8318.
35. Demers, L. M.; Mirkin, C. A.; Mucic, R. C.; Reynolds, R. A.; Letsinger, R. L.; Elghanian, R.; Viswanadham, G. A Fluorescence-Based Method for Determining the Surface Coverage and Hybridization Efficiency of Thiol-Capped Oligonucleotides Bound to Gold Thin Films and Nanoparticles. *Anal. Chem.* **2000**, *72*, 5535–5541.
36. Palegrosdemange, C.; Simon, E. S.; Prime, K. L.; Whitesides, G. M. Formation of Self-Assembled Monolayers by Chemisorption of Derivatives of Oligo(ethylene glycol) of Structure $HS(CH_2)_{11}(OCH_2CH_2)_m$-OH on Gold. *J. Am. Chem. Soc.* **1991**, *113*, 12–20.
37. Liu, J. W.; Lu, Y. Optimization of a Pb^{2+}-Directed Gold Nanoparticle/DNAzyme Assembly and Its Application as a Colorimetric Biosensor for Pb^{2+}. *Chem. Mater.* **2004**, *16*, 3231–3238.
38. Zaborowska, Z.; Furste, J. P.; Erdmann, V. A.; Kurreck, J. Sequence Requirements in the Catalytic Core of the "10-23" DNA Enzyme. *J. Biol. Chem.* **2002**, *277*, 40617–40622.
39. Richards, J. L.; Seward, G. K.; Wang, Y. H.; Dmochowski, I. J. Turning the 10-23 DNAzyme On and Off with Light. *ChemBioChem* **2010**, *11*, 320–324.
40. Jain, P. K.; Shah, S.; Friedman, S. H. Patterning of Gene Expression Using New Photolabile Groups Applied to Light Activated RNAi. *J. Am. Chem. Soc.* **2010**, *133*, 440–446.
41. Prokup, A.; Hemphill, J.; Deiters, A. DNA Computation: A Photochemically Controlled AND Gate. *J. Am. Chem. Soc.* **2012**, *134*, 3810–3815.
42. Poon, L.; Zandberg, W.; Hsiao, D.; Erno, Z.; Sen, D.; Gates, B. D.; Branda, N. R. Photothermal Release of Single-Stranded DNA from the Surface of Gold Nanoparticles through Controlled Denaturating and Au−S Bond Breaking. *ACS Nano* **2010**, *4*, 6395–6403.
43. Young, D. D.; Lively, M. O.; Deiters, A. Activation and Deactivation of DNAzyme and Antisense Function with Light for the Photochemical Regulation of Gene Expression in Mammalian Cells. *J. Am. Chem. Soc.* **2010**, *132*, 6183–6193.
44. Zhou, M. G.; Liang, X. G.; Mochizuki, T.; Asanuma, H. A Light-Driven DNA Nanomachine for the Efficient Photoswitching of RNA Digestion. *Angew. Chem., Int. Ed.* **2010**, *49*, 2167–2170.
45. Bootcov, M. R.; Bauskin, A. R.; Valenzuela, S. M.; Moore, A. G.; Bansal, M.; He, X. Y.; Zhang, H. P.; Donnellan, M.; Mahler, S.; Pryor, K.; *et al.* MIC-1, A Novel Macrophage Inhibitory Cytokine, Is a Divergent Member of the TGF-Beta Superfamily. *Proc. Natl. Acad. Sci. U.S.A.* **1997**, *94*, 11514–11519.
46. Welsh, J. B.; Sapinoso, L. M.; Kern, S. G.; Brown, D. A.; Liu, T.; Bauskin, A. R.; Ward, R. L.; Hawkins, N. J.; Quinn, D. I.; Russell, P. J.; *et al.* Large-Scale Delineation of Secreted Protein Biomarkers Overexpressed in Cancer Tissue and Serum. *Proc. Natl. Acad. Sci. U.S.A.* **2003**, *100*, 3410–3415.
47. Staff, A. C.; Bock, A. J.; Becker, C.; Kempf, T.; Wollert, K. C.; Davidson, B. Growth Differentiation Factor-15 as a Prognostic Biomarker in Ovarian Cancer. *Gynecol. Oncol.* **2010**, *118*, 237–243.
48. Chang, J. T.-C.; Chan, S.-H.; Lin, C.-Y.; Lin, T.-Y.; Wang, H.-M.; Liao, C.-T.; Wang, T.-H.; Lee, L.-Y.; Cheng, A.-J. Differentially Expressed Genes in Radioresistant Nasopharyngeal Cancer Cells: gp96 and GDF15. *Mol. Cancer Ther.* **2007**, *6*, 2271–2279.
49. Joshi, J. P.; Brown, N. E.; Griner, S. E.; Nahta, R. Growth Differentiation Factor 15 (GDF15)-Mediated HER2 Phosphorylation Reduces Trastuzumab Sensitivity of HER2-Overexpressing Breast Cancer Cells. *Biochem. Pharmacol.* **2011**, *82*, 1090–1099.
50. Nahta, R.; Esteva, F. J. Herceptin: Mechanisms of Action and Resistance. *Cancer Lett.* **2006**, *232*, 123–138.
51. Hill, H. D.; Mirkin, C. A. The Bio-Barcode Assay for the Detection of Protein and Nucleic Acid Targets Using DTT-Induced Ligand Exchange. *Nat. Protoc.* **2006**, *1*, 324–336.
52. Sato, K.; Hosokawa, K.; Maeda, M. Rapid Aggregation of Gold Nanoparticles Induced by Non-Cross-Linking DNA Hybridization. *J. Am. Chem. Soc.* **2003**, *125*, 8102–8103.